Molecular Structure Influences the Stability of Membrane Penetrating Bio-Interfaces.

*Benjamin D. Almquist & Nicholas A. Melosh**

Department of Materials Science and Engineering, Stanford University, Stanford, CA 94305

*nmelosh@stanford.edu

ABSTRACT. Nanoscale patterning of hydrophobic bands on otherwise hydrophilic surfaces allows integration of inorganic structures through biological membranes, reminiscent of transmembrane proteins. Here we show that a set of innate molecular properties of the self-assembling hydrophobic band determine the resulting interface stability. Surprisingly, hydrophobicity is found to be a secondary factor, with monolayer crystallinity the major determinate of interface strength. These results begin to establish guidelines for seamless bio-inorganic integration of nanoscale probes with lipid membranes.

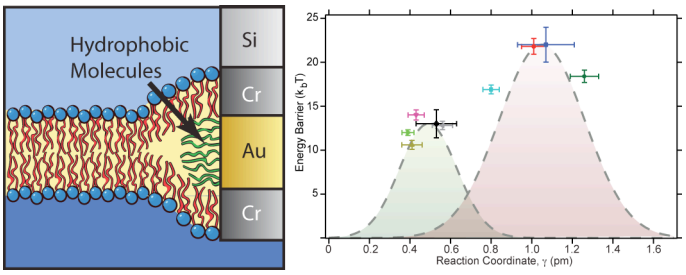

KEYWORDS. Atomic Force Microscopy, Biophysics, Biological Interfaces, Lipid Membranes

MANUSCRIPT TEXT. Cellular membranes are dynamic, nanostructured thin films that present a formidable barrier to biotic/abiotic integration. These membranes prevent passage of most polar molecules between the intracellular and extracellular space,[1] and maintaining their integrity is key to

preserving normal cellular function. Recently, there has been a push to develop devices that can artificially measure and control electrical and chemical transfer across the membrane.[2-7] In many cases, nanostructures are being utilized for membrane penetration due to improvements in cell viability. However, penetration is generally a transient process and enabling long-term measurements remains elusive.

In order to facilitate long-term membrane integration, new insight into cell membrane-material interfaces is necessary. Detrimental membrane perturbation may be avoidable if penetrating materials interact specifically with the 3 distinct nanoscale zones found while spanning the 5-6nm thick lipid bilayer: the upper water and hydrophilic lipid headgroups, the hydrophobic bilayer core (~3nm thick), and the lower hydrophilic lipid headgroups. (Fig. 1a).[8] Transmembrane proteins display similar hydrophobic patterning, which enables ionically tight interface formation.[9] To form stable, high-quality bio-inorganic interfaces, each of these regions ought to be correctly matched, replicating the design of endogenous proteins. Recent work has found that nanoparticles with mixed-hydrophobicity at the Ångstrom level allow particles to slip through the bilayer directly,[5] but such patterning is likely not ideal for promoting long-term integration.

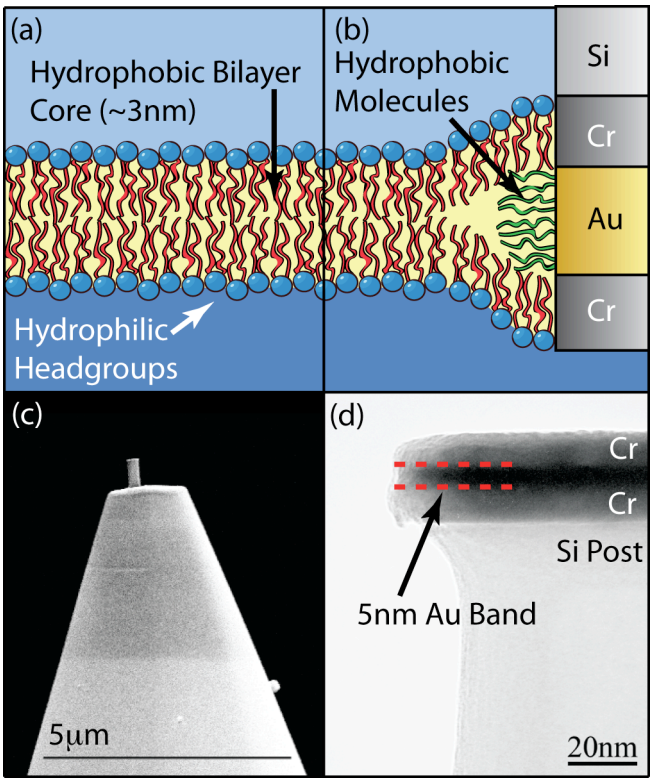

Figure 1. (a) Structure of a lipid bilayer. Surfaces are composed of hydrophilic headgroups while the core is composed of hydrophobic acyl chains. (b) Stealth probe geometry. (c) SEM image of a stealth probe at the end of an AFM tip. (d) TEM image of metallic stack with a 5nm Au band at the end of a stealth probe.

We have recently applied the design rules garnered from transmembrane proteins to design inorganic posts with 2-10 nm hydrophobic bands on otherwise hydrophilic structures.[10, 11] These devices rely on exposing the edge of an embedded Au layer, which is sandwiched between metal layers that possess a hydrophilic oxide (e.g. Cr, Ti). The exposed Au edge is subsequently functionalized with a thiol-based, hydrophobic self-assembled monolayer (Fig. 1b,c,d). This hydrophobic functional band encourages specific insertion into the hydrophobic membrane core, and can form well-defined, stable interfaces. Experiments with these 'stealth' probes showed spontaneous fusion into lipid bilayer cores, and formation of tight membrane interfaces with electrical resistances over 3 GΩ.[6]

One of the most critical aspects of this architecture is understanding how the characteristics of the probe design influence the membrane-inorganic interface. Bio-hydrophobicity scales have been

developed to predict whether certain peptide sequences are likely to partition into the hydrophobic bilayer core.[12] However, for artificial systems the range of possible materials is much broader than amino acids, such that new criteria may become relevant. The stealth probe design provides the ability to modulate both the thickness of the hydrophobic band by tuning the Au thickness, and the molecular structure of the self-assembled monolayer on its surface. We previously found that the Au band thickness strongly influences the membrane-probe adhesion strength, in good agreement with predictions from membrane deformation models.[11] Here we examine how different molecular functionalizations influence the membrane-probe interface. Initial results found that butanethiol possesses a superior interfacial strength compared to dodecanethiol,[10] thus we chose to explore a series of alkanethiols and closely related molecules.

Atomic force microscopy (AFM) force clamp spectroscopy was used to measure the effect of different stealth probe functionalizations. Unlike far-field techniques such as fluorescence and X-ray scattering, this method provides dynamic information regarding the probe location within a bilayer and quantitative measurement of the bilayer-probe interfacial strength.[10]

AFM cantilevers with a Cr/Au/Cr stack located at the tip were fabricated using a combination of metal deposition and focused ion beam (FIB) milling. This procedure, which is described in detail elsewhere,[10, 11] results in cantilevers with ~200nm posts at the tip that contain a 5nm Au band (Fig. 1b,d). These modified stealth probes were then functionalized by immersing in ethanol solutions of 5mM butane-, hexane-, octane-, decane-, dodecane-, or hexadecanethiol for four hours.

Functionalized stealth probes were subsequently tested using force clamp spectroscopy by bringing the tip into contact with a lamellar stack of 2:1 SOPC:cholesterol lipid bilayers, and rapidly ramping the applied force to a large value of ~≤80nN. The z-piezo position is then fixed, at which point the accumulated load is relieved by the probe tip breaking through the lipid bilayers. Breakthrough occurs when failure occurs at the membrane-probe interface and in the underlying lipid bilayer (Fig. 2a). Depending on the strength of the bio-inorganic interface, either mechanism can be the rate-limiting step.

The resulting curves of tip displacement vs. force form characteristic stair-step patterns, as shown in Fig. 2b. In these curves, the sharp vertical drops correspond to penetration of a lipid bilayer while the horizontal plateaus correspond to the tip loading a fresh bilayer in the stack. The data from a number of curves is compiled to determine the average breakthrough rate for a given force.

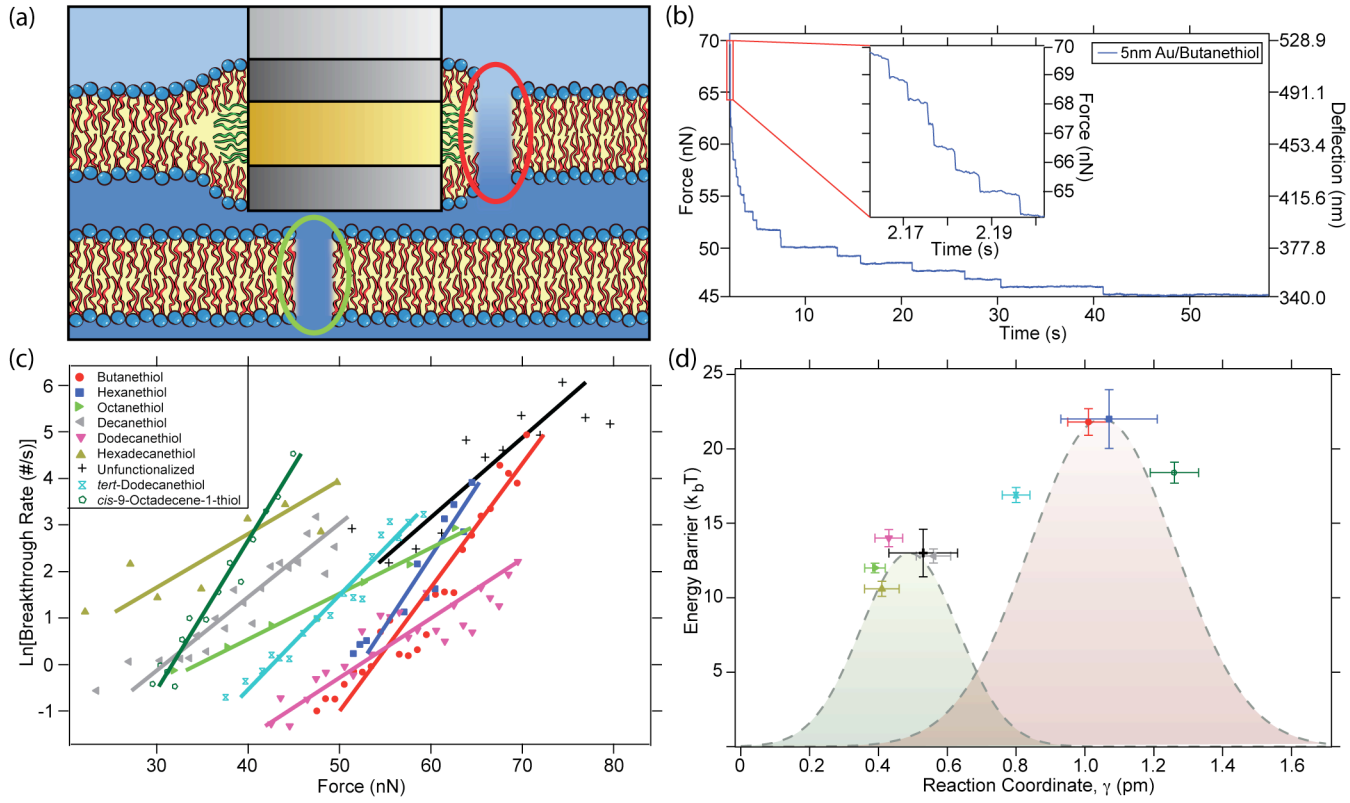

Figure 2. (a) Schematic of defect nucleation sites during force clamp testing: at the membrane-probe interface (red circle) and in the bilayer underneath the stealth probe tip (green circle). (b) Force clamp testing curve. Vertical drops correspond to breaking though one bilayer followed by horizontal plateaus while the tip loads a fresh bilayer. (c) Linear fits of *ln(k)* as a function of breakthrough force for each stealth probe functionalization. (d) Plot of energy barrier height E_0 and reaction coordinate γ derived from part (c). Failure rate for high strength functionalizations is limited by defect generation at the membrane-probe interface (red Gaussian). Unfunctionalized and low strength functionalizations are limited by defect generation in the underlying lipid bilayer (green Gaussian). Gaussians are schematic representations to help visualize energy barrier locations.

In these experiments, each of the failure events (membrane-probe interface failure, underlying bilayer penetration) can be represented as an energy-barrier crossing event within a Langevin reaction model under an applied force.[13] Since these events occur in separate bilayers and are unlikely to involve a coordinated failure mechanism, the energy barrier measured during bilayer failure will reflect the larger of the two energy barriers at a given force. These energy barriers can be directly calculated from the breakthrough (failure) rate k at different applied forces F using:

$$k = A\exp\left(-\frac{E_o - F\gamma}{k_b T}\right) \qquad [1]$$

$$\ln(k) = F\left(\frac{\gamma}{k_b T}\right) - \left(\frac{E_0}{k_b T} - \ln(A)\right) \qquad [2]$$

where A is the attempt frequency (the cantilever resonance of ~6 kHz was used)[14], E_0 is the unstressed energy barrier height, T is the absolute temperature, and γ relates how much the applied force influences the energy barrier height. In molecular reaction theory γ is the location of the energy barrier maximum along the reaction coordinate. In larger systems it is the stress (force per unit area) rather than the total force that determines the failure at a particular location. The effective area is often implicitly included in γ, such that its value no longer reflects molecular phenomena. In these measurements γ roughly ranges from 0.4 to 1.3 pm (Table 1), which when adjusted over the ~1800 lipids at the probe interface gives a per-molecule value of 0.7 to 2.3 nm, comparable to values for SOPC lipid pullout from bilayer vesicles.[15] In our experiments the interpretation of the per-molecule γ will depend upon whether the rate-limiting failure occurs at the probe tip or at the functionalized band, but approximately represents the molecular strain at failure.

The energy barrier E_0 and γ for the various functional band chemistries was determined by fitting *ln(k)* according to Eq. 2, with the results shown in Fig. 2c and Table 1. Unfunctionalized probes were

first measured to determine E_0 and γ for the situation where penetration of the underlying bilayer is the rate-limiting step, rather than bilayer adhesion to the band. The energy barrier height of 13.0±1.6k_bT for the unfunctionalized case is in excellent agreement with the previously reported[16] energy barrier for defect formation and failure in SOPC bilayers of ~13.6k_bT.

The measured energy barriers for the functionalized stealth probes show a dramatic dependence on alkanethiol length. The two shortest alkanethiols (butanethiol, hexanethiol) have a high average E_0 of 21.9k_bT and γ of 1.04pm, indicating that it is difficult to pull these molecules out of the hydrophobic bilayer core, and thus have strong adhesion strength. However, the barrier energy and γ values for octanethiol or longer alkanes drops precipitously, and in fact appears to be equal to or smaller than unfunctionalized probes. The energy barrier does not vary linearly with alkane length, but instead shows two distinct regimes with the transition between six and eight carbon long alkanes.

Plotting E_0 vs γ for the different functionalizations reveals the position of the unstressed energy barrier maxima and clearly distinguishes between the two rate-limiting failure processes (Fig. 2d). During testing, the applied force reduces the height of these barriers by $F\gamma$. The differences in γ make it possible for the dominant energy barrier to change during testing, however this is not observed here. Failure of butanethiol and hexanethiol probes is governed by a barrier located at large γ, which corresponds to failure at the membrane-probe interface. Meanwhile, longer chain alkanethiols have smaller resistance to bilayer removal than the barrier to penetrate the underlying bilayer, and have the same E_0 and γ as unfunctionalized probes. The significant shift in E_0 and γ to the unfunctionalized values indicates that failure in the lower bilayer has become the rate-limiting step rather than failure at the functionalized interface. However, a limitation on the range of testing forces restricts our ability to accurately determine the interface strength for these longer chains. It is possible, though, to estimate the upper bound of the unstressed interface energy barrier by assuming a γ equal to that of the short chain alkanes, and was found to be approximately 16k_bT.

Molecular Functionalization	E_f	γ
	k_bT	pm
Butanethiol	21.8 ± 0.9	1.01 ± 0.06
Hexanethiol	22.0 ± 2.0	1.07 ± 0.14
Octanethiol	12.0 ± 0.3	0.39 ± 0.03
Decanethiol	12.8 ± 0.5	0.56 ± 0.05
Dodecanethiol	14.0 ± 0.6	0.43 ± 0.04
Hexadecanethiol	10.6 ± 0.5	0.41 ± 0.05
Unfunctionalized	13.0 ± 1.6	0.53 ± 0.10
tert-Dodecanethiol	16.9 ± 0.5	0.80 ± 0.04
cis-9-Octadecene-1-thiol	18.4 ± 0.7	1.26 ± 0.07

Table 1. E_0 and γ for the various molecular functionalizations.

To uncover the underlying cause for the abrupt change in dominant failure mechanism, we examined other properties of the system. Fig. 3 compares the E_0 values (Fig. 3a) to the measured breakthrough distances (Fig. 3b), water contact angles (Fig. 3c, circles) and hexadecane contact angles (Fig. 3c, squares) for each functionalization. The breakthrough distances, which reflect the center-to-center distance between bilayers, remain relatively consistent over the alkanethiol series with an average of 5.7±0.3nm, and do not show any abrupt changes. We can thus rule out changes in the penetration mechanism or measurement technique that might create this effect. [10]

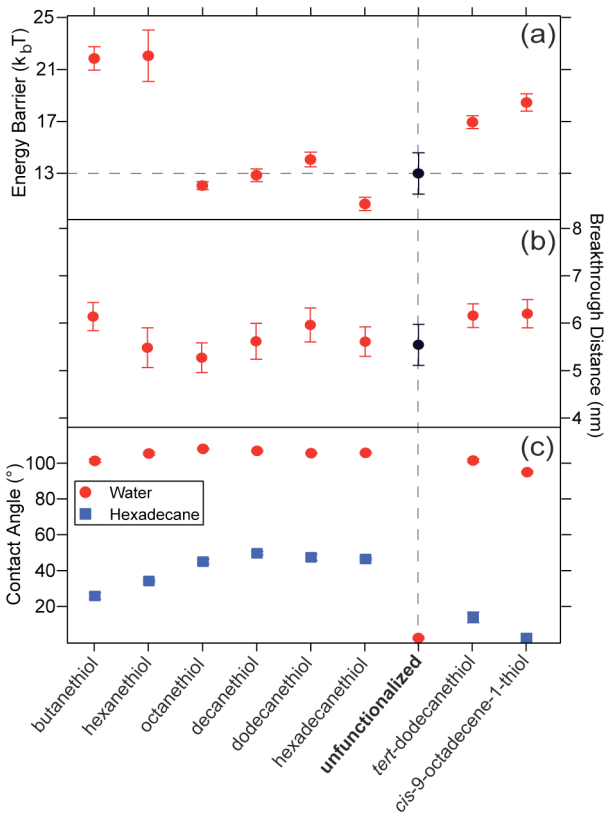

Figure 3. Plot of the measured (a) energy barrier heights, (b) breakthrough distances, and (c) contact angles (circles, water; squares, hexadecane) for each functionalization. Breakthrough distances are measured to determine if changes in functionalization alter the penetration process, while the water and hexadecane contact angles measure the hydrophobicity and oleophilicity of the functionalizations, respectively.

Moreover, the change in adhesion strength is not directly linked to a change in monolayer hydrophobicity. Water contact angles are greater than 100° for all alkanethiol lengths, and hexanethiol and octanethiol are only different by ~2%. Hexadecane contact angles reflect the alkane oleophilicty (indicated by low hexadecane contact angles), and show slight increases for butanethiol and hexanethiol. While these surface energy effects may play some role in the change in strength, these energies vary smoothly over the alkane series without any sudden jumps that could account for the sharp transition observed.

However, previous studies using ellipsometry and IR spectroscopy have shown that alkanethiol self-assembled monolayers display an abrupt transition from a fluid to a crystalline phase between hexanethiol and octanethiol.[17] This suggests the weakening of the membrane-stealth probe interface is due to the crystallinity of the molecular surface, with fluid, disordered monolayers promoting a high strength interface regime, and rigid, crystalline SAMs forming weak interfaces.

To test this hypothesis, it is necessary to decouple monolayer crystallinity from other molecular properties. Inherent in the linear alkanethiol measurements is the fact that crystallization is linked to increasing molecular length. To separate these two properties, stealth probes were functionalized with either *cis*-9-octadecene-1-thiol or an isomeric mixture of *tert*-dodecanethiol. In each of these cases, the monolayers are sterically hindered from crystallizing. A kink in the carbon chain due to the presence of a C=C double bond prevents *cis*-9-octadecene-1-thiol from forming a close-packed monolayer. These molecules have a relatively low water contact angle of 94.9±0.6° and <10° with hexadecane. Similarly, *tert*-dodecanethiol possesses two methyl side groups that hinder the close packing necessary for crystallization, with a water contact angle of 101.5±1.0° and a hexadecane contact angle of 14.0±3.0°. In each case, it is hypothesized that the membrane-probe interface will be stronger than similar length straight chain alkanes due to the lack of crystallinity.

Results from force clamp testing confirm this hypothesis, with *cis*-9-octadecene-1-thiol and *tert*-dodecanethiol displaying strengths of E_o=18.4±0.7k_bT and E_o=16.9±0.5k_bT, respectively. Both of these values are higher than the equivalent sized linear alkane and show a γ values near 1 pm, consistent with failure at the functionalized interface. Crystallinity thus appears to be a major factor in interfacial strength. While substantially stronger than crystalline alkanethiols, both functionalizations are weaker than the shorter butanethiol and hexanethiol monolayers. This suggests that the stability of these interfaces is also influenced by other physiochemical properties.

Interestingly, it appears that hydrophobicity is only a secondary factor in determining interface strength. As seen in Fig. 3, the most hydrophilic monolayer (*cis*-9-octadecene-1-thiol) provides a

stronger interface than the most hydrophobic ones (crystalline alkanethiol monolayers). However, this observation should not be used to overlook the importance of the molecular scale configuration; previous work has shown that hydrophobicity drives spontaneous insertion into the bilayer core.[10] Once integrated inside the bilayer, though, other molecular properties seem to determine the interfacial strength. The results presented here suggest monolayer crystallinity and molecular size (properties that influence the intermolecular interactions at the probe-bilayer interface) all contribute to the overall interfacial strength.

Monolayer crystallinity displays the most direct correlation with interface strength, potentially due to changes in the magnitude of van der Waals bonding across the interface. Crystalline alkanethiol monolayers possess methyl-terminated surfaces, while disordered monolayers can also expose underlying methylene groups. While methyl groups are intrinsically more polarizable than methylene,[18] the polarizability of methylene groups is approximately 16% larger after accounting for differences in volume.[19] Trends in oleophilicity support this; surfaces with larger ratios of methyl to methylene result in larger alkane contact angles.[20] In addition, crystallization diminishes alkanethiol mobility, reducing the ability of the alkanethiols to reorient and maximize van der Waals bonding. Furthermore, crystallized monolayers may cause a significant reduction in the entropy of the lipid acyl chains, although further work is necessary to fully explore the molecular-level details of the interfacial region. Nevertheless, the force clamp data demonstrates that crystalline, methyl-terminated surfaces form penetrating biointerfaces with low strength, in agreement with adhesion testing.[10]

The results presented here also indicate a dependence on molecule size and microscopic geometry. If the magnitude of van der Waals bonding was the sole component contributing to interface stability, it is thought that *tert*-dodecanethiol and *cis*-9-octadecene-1-thiol would both display stronger interfaces than the alkanethiol series. While they do display improved interfacial strengths compared to crystalline monolayers, they display lower interfacial strengths than butanethiol and hexanethiol.

Molecular size may contribute to interfacial strength due to limits on the amount of free volume

available in the hydrophobic bilayer core. It is known that lipid-chain ordering decreases at the bilayer midplane.[8] While there exists a large amount of free volume at the bilayer midplane, acyl chain regions closer to the lipid phosphate group are more ordered and compact, with the presence of cholesterol enhancing this property.[21] Since the 5nm molecular layer must interact with the full thickness of the bilayer core, the functional molecules must be able to integrate into regions of both high and low free volume, and thus favor the use of short molecules.

The combination of molecular mobility and limited free volume may have implications on the ordering of molecules in fluid functional bands. Studies have shown that alkanes shorter than heptane preferentially reside in the disordered bilayer midplane, while longer alkanes orient parallel to the lipid acyl chains.[22-25] In the case of the stealth probes, alkanethiol molecules are fixed in position due to the thiol linkage, limiting their ability to adopt the preferred orientation. Due to this constraint, it is hypothesized that near the edges of the functional band, molecules likely attempt to orient parallel to lipid acyl chains (Fig. S1). Limited free volume and reduced entropic freedom along with increased van der Waals bonding are thought to drive this reorientation. Meanwhile, as the bilayer midplane is approached, molecules likely transition to a more perpendicular orientation to take advantage of the increase in free volume and decrease in van der Waals bonding.[26]

Combining these various phenomena, the strength of penetrating material-bilayer interfaces is dependent on a set of molecular properties. Suprisingly, monolayer crystallinity displays the largest correlation with interface strength, with hydrophobicity and oleophilicity existing as secondary factors. By transitioning from a crystalline to disordered monolayer, more polarizable methylene groups are exposed and the molecules are allowed to reorient to increase van der Waals interaction. However, the desire to maximize van der Waals bonding is constrained by limited free volume within the bilayer core for functional molecule incorporation.

In summary, we have demonstrated that biomimetic stealth probes that possess nanoscale hydrophobic bands fuse into lipid bilayers, forming tunable bio-inorganic interfaces. Maximum

interface strength was obtained with short, fluid-phase alkanethiols, with increases in molecular length and monolayer crystallinity resulting in interface destabilization. These results replicate key observations of transmembrane protein structure, and begin to establish a set of design guidelines for biotic/abiotic interface formation.

ACKNOWLEDGMENTS. This work was performed using equipment that was supported [in part] by the Department of Energy, Office of Basic Energy Sciences, Division of Materials Sciences and Engineering, under contract DE-AC02-76SF00515. Funding was also provided by the NSF Center for Probing the Nanoscale grant No. PHY-0425897, and B.D.A. acknowledges the NSF CPN for fellowship support.

REFERENCES:

1. Alberts, B.; Johnson, A.; Lewis, J.; Raff, M.; Roberts, K.; Walter, P., *Molecular Biology of the Cell, 4th Ed*. Taylor & Francis Group: New York, NY, 2002.

2. Kim, W.; Ng, J. K.; Kunitake, M. E.; Conklin, B. R.; Yang, P. *J. Am. Chem. Soc*. **2007,** 129, (33), 7228-7229.

3. Schrlau, M. G.; Bau, H. H. *Microfluid Nanofluid* **2009,** 7, 439-450.

4. Tian, B.; Cohen-Karni, T.; Qing, Q.; Duan, X.; Xia, P.; Lieber, C. M. *Science* **2010,** 329, 830-834.

5. Verma, A.; Uzun, O.; Hu, Y.; Hu, Y.; Han, H.-S.; Watson, N.; Chen, S.; Irvine, D. J.; Stellacci, F. *Nature Materials* **2008,** 7, 588-595.

6. Verma, P.; Melosh, N. A. *Applied Physics Letters* **2010,** 97, (3), 033704-3.

7. Yum, K.; Wang, N.; Yu, M.-F. *Nanoscale* **2010,** 2, 363-372.

8. Nagle, J. F.; Tristram-Nagle, S. *Biochimica et Biophysica Acta (BBA) - Reviews on Biomembranes* **2000,** 1469, (3), 159-195.

9. Lee, A. G. *Biochim. Biophys. Acta, Biomembr.* **2003,** 1612, 1-40.

10. Almquist, B. D.; Melosh, N. A. *Proc. Natl. Acad. Sci., U.S.A.* **2010,** 107, (13), 5815-5820.

11. Almquist, B. D.; Verma, P.; Cai, W.; Melosh, N. A. *Nanoscale* **2011,** 3, 391-400.

12. Wimley, W. C.; White, S. H. *Nat. Struct. Biol.* **1996,** 3, (10), 842-848.

13. Evans, E.; Ritchie, K. *Biophys. J.* **1997,** 72, 1541-1555.

14. Loi, S.; Sun, G.; Franz, V.; Butt, H.-J. *Phys. Rev. E.* **2002,** 66, 031602.

15. Evans, E.; Ludwig, F. *J. Phys.: Condens. Matter* **2000,** 12, A315-A320.

16. Evans, E.; Heinrich, V.; Ludwig, F.; Rawicz, W. *Biophys. J.* **2003,** 85, 2342-2350.

17. Porter, M. D.; Bright, T. B.; Allara, D. L.; Chidsey, C. E. D. *Journal of the American Chemical Society* **1987,** 109, (12), 3559-3568.

18. Miller, K. J. *J. Am. Chem. Soc.* **1990,** 112, 8533-8542.

19. Bader, R. F. W.; Carroll, M. T.; Cheeseman, J. R.; Chang, C. *J. Am. Chem. Soc.* **1987,** 109, 7968-7979.

20. Fox, H. W.; Zisman, W. A. *Journal of Colloid Science* **1952,** 7, (4), 428-442.

21. Hung, W.-C.; Lee, M.-T.; Chen, F.-Y.; Huang, H. W. *Biophys. J.* **2007,** 92, 3960-3967.

22. Haydon, D. A.; Hendry, B. M.; Levinson, S. R. *Nature* **1977,** 268, 356-358.

23. Haydon, D. A.; Hendry, B. M.; Levinson, S. R.; Requena, J. *Biochem. Biophys. Acta* **1977,** 470, 17-34.

24. McIntosh, T. J.; Simon, S. A.; MacDonald, R. C. *Biochem. Biophys. Acta* **1980,** 597, 445-463.

25. White, S. H.; King, G. I.; Cain, J. E. *Nature* **1981,** 290, 161-163.

26. MacCallum, J. L.; Tieleman, D. P. *J. Am. Chem. Soc.* **2006,** 128, 125-130.

SUPPORTING INFORMATION.

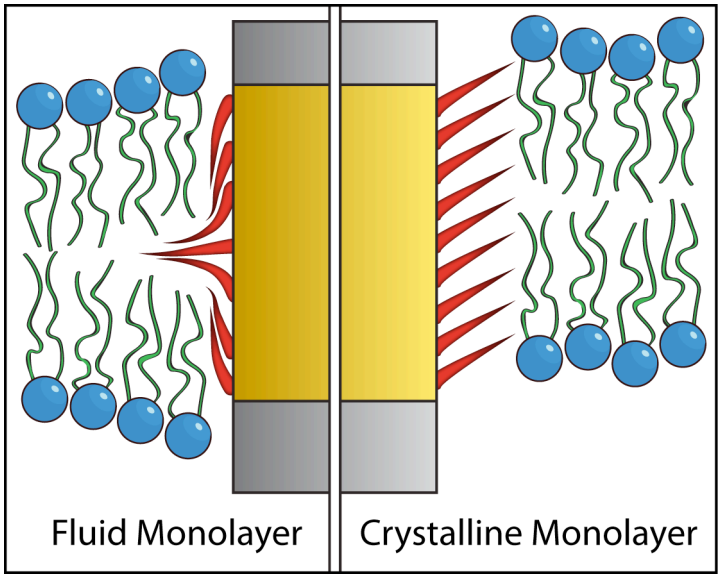

Figure S1. (left) Fluid monolayers likely have an orientational gradient in order to take advantage of changes in free volume present throughout the hydrophobic bilayer core, whereas crystalline monolayers (right) are unable to reorganize in response to the bilayer structure.